

6-dimensional localized black holes: numerical solutions

Hideaki Kudoh

Department of Physics, Kyoto University, Kyoto 606-8502, Japan

To test the strong-gravity regime in Randall-Sundrum braneworlds, we consider black holes bound to a brane. In a previous paper, we studied numerical solutions of localized black holes whose horizon radii are smaller than the AdS curvature radius. In this paper, we improve the numerical method and discuss properties of the 6D localized black holes whose horizon radii are larger than the AdS curvature radius. At a horizon temperature $T = 2/\ell$, the thermodynamics of the localized black hole undergo a transition with its character changing from a 6D Schwarzschild black hole type to a 6D black string type. The entropy of the localized black holes is greater than or nearly equal to that of the 6D black strings with the same thermodynamic mass. Large localized black holes show flattened horizon geometries, and the intrinsic curvature of the horizon 4-geometry becomes negative near the brane.

PACS numbers: 04.50.+h, 04.70.Dy, 04.70.Bw, 11.25.Wx

I. INTRODUCTION

Much progress has been made in understanding the dynamics of gravity, brane and localized matter fields in the context of braneworlds. The braneworld models proposed by Randall and Sundrum (RS) [1, 2] have an extra dimension which is compactified via anti-de Sitter (AdS) space and branes, assuming that we live on a brane (or a domain wall) inside the AdS space. This compactification is called warped compactification. The RS models do not require a large extra dimension due to the warped compactification, contrary to other interesting braneworld models with large extra dimensions [3, 4].

In the warped compactification, analyses of linear and second-order perturbations show that gravity induced on the brane by localized matter fields is consistent with usual 4-dimensional Einstein gravity [5, 6, 7, 8, 9, 10, 11, 12, 13, 14], although the problem is essentially 5-dimensional. For the strong-gravity regime in the RS models, the low energy (or derivative) expansion method would be a useful approach in some cases [15, 16, 17]. A recent fully non-linear numerical treatment of time-dependent braneworld models is also an interesting development to understand nonlinear brane dynamics [18].

A pioneering approach to strongly gravitating systems in the RS model is developed by Wiseman in the study of relativistic stars on the brane [19]. In this study, the full 5-dimensional Einstein equations are solved numerically, employing a conformal gauge method that reduces the Einstein equations to a suitable boundary value problem under an assumption of static axisymmetry. A consequence of nonlinear effects in standard 4-dimensional Einstein gravity is the existence of an upper mass limit at fixed radius of relativistic stars. The existence of the upper mass limits is confirmed for small stars whose proper radii R are less than the AdS curvature radius ℓ . While the upper mass limits for large stars whose radii are $R \gg \ell$ are not confirmed, all observed physical quantities indicate that an effective 4-dimensional description by means of 4-dimensional Einstein gravity applies far into the nonlinear regime. Then so-called recovery mechanism of Einstein gravity on the brane would persist in the strong-gravity regime.

The basic idea of the conformal gauge method is a key to explore the nonlinear regime of gravity with extra dimensions. Indeed, it has been applied for non-uniform black strings [20, 21] and Kaluza-Klein black holes [22, 23]. As is emphasized in Ref. [20], the problem of non-uniform black strings is a clean and simple application of the conformal gauge method compared with the other applications, due to a technical issue of numerics associated with the coordinate system at the symmetry axis (see, e.g., Ref. [24, 25] for a similar problem in numerical relativity, although the technical issue is intrinsic to the conformal gauge).

The method is also applied to a study of black holes in the RS braneworld model [26, 27]. Physically realistic black holes are thought to localize on the brane, as matter fields localize there [8]. Static axisymmetric localized black holes, for example, would be formed as a result of gravitational collapse on the brane, settling down to a static state at late times. There are many discussions about the localized black holes [28, 29, 30, 31, 32, 33, 34, 35, 36, 37, 38, 39, 40, 41, 42] (recent discussions are [43, 44, 45, 46]). However, physically acceptable black hole solutions have not been found so far, except for exact solutions in the 4-dimensional RS braneworld found by Emparan, Horowitz and Myers

Electronic address: kudoh@yukawa.kyoto-u.ac.jp

(EHM) [47, 48]. An interesting argument motivated by a no-go theorem [49] and the AdS/CFT correspondence in the RS braneworld (e.g. [50, 51]) is that large localized static black holes may not exist [52, 53].

In our previous papers, we considered the localized black holes in 5-dimensional RS single brane model, and presented some examples of numerical solutions [26, 27]. However, we could not succeed in constructing localized black holes that are larger than the AdS radius, because the numerical scheme gave no convergent solution for them. To overcome the difficulty and to obtain an understanding of localized black holes, we need further development of the method. A key method had been developed through the study of Kaluza-Klein black holes [22] (see also Ref. [19]). In this paper, we apply the improved numerics and discuss numerical solutions of static localized black holes. We perform the analysis in the 6-dimensional RS model. This is just a technical reason that numerical calculations in higher dimensions have an advantage. The metric in higher dimensions decay faster than that in the original 5-dimensional braneworld model and then it makes numerical calculations more tractable [20]. We think that there is no qualitative difference between localized black holes in 5-dimensions and those in 6-dimensions. Indeed, as we will see, thermodynamic properties of the small localized black holes in 5-dimensions found in Ref. [26, 27] persist in 6-dimensions. While the EHM solutions are known in 4-dimensions, the difference between 4-dimensions and more than 4 is very large. For example, the EHM black holes have a maximum mass that is an outcome of the deficit angle in the spacetime.

We are interesting in qualitative properties of the localized black holes, for example, thermodynamic property, horizon geometry and gravity induced on the brane. In particular, it is an interesting question whether the lower dimensional Einstein gravity is recovered on the brane even in the presence of a localized black hole. We construct the static localized black holes by means of the numerical method and discuss the fundamental properties of the black holes.

In Section II, we begin by briefly reviewing the conformal gauge method, and then in Section III, we present numerical solutions, showing the performance of the method. Properties of the localized black holes and their implications are discussed in Section IV. Section V is devoted to a summary. Due to the technical nature of Section III, the reader may prefer to skip straight to Section IV.

II. 6-DIMENSIONAL BRANEWORLD BLACK HOLES

A. Conformal gauge method

Following the previous work [26, 27], we adopt the conformal gauge method to construct localized black holes. We begin with a general ansatz for static axisymmetric black hole solutions to Einstein's equations with a bulk cosmological constant in D -dimensions.

$$ds^2 = \frac{r^2}{z^2} \left(-e^2 dt^2 + e^2 (dr^2 + dz^2) + r^2 e^2 d\Omega_{D-3}^2 \right); \quad (1)$$

where the metric functions are arbitrary functions of r and z . The bulk cosmological constant is $\Lambda = (D-1)(D-2)/2$; and tension of the branes is $\sigma = 2(D-2)/D$. Here $D = 8$, G_D is D -dimensional Newton's constant and ℓ is the AdS curvature radius. Israel's junction condition at the brane in D -dimensions gives $K_{ij} = \sigma \gamma_{ij}$; where K is the extrinsic curvature of the brane at $z = \ell$ with the induced metric γ_{ij} .

Now we consider six-dimensional (6D) single brane model. The metric form has the residual gauge degrees of freedom of conformal transformations in the two-dimensional space $fr;zg$, and then we can use these conformal degrees of freedom to transform the location of the event horizon to be at a constant radius

$$r = r_0; \quad (2)$$

Here we have introduced polar coordinates,

$$\begin{aligned} r &= r_0 \sin \theta; \\ z &= \ell + r_0 \cos \theta; \end{aligned} \quad (3)$$

Note that the positive tension brane can be placed at $z = \ell$. We introduce

$$u = \theta^2; \quad (4)$$

This variable is used in Ref. [26] to gain numerical stability near the axis. However even with this modification, the algorithm is still unstable and encounters lack of convergence when we increase the radius of black hole. As we

discuss later, this numerical problem is resolved in Ref. [22], altering a method originally used in Ref. [19]. An aim in using the variable (4) is to increase a numerical resolution near the brane. All numerical calculations presented in this paper are performed by using the variable (4)¹.

If the localized black hole is sufficiently small compared to the curvature radius in the bulk, the black hole would be approximated by the 6D Schwarzschild black hole because the tension of the brane and the bulk cosmological constant would not affect locally the black hole. This is in fact observed in the study of 5D braneworld black holes [27]. Thus we subtract the 6D Schwarzschild metric from the assumed metric. Rewriting the metric functions as [26]

$$\begin{aligned} &= A_0; \\ &= B_0 - C_0; \\ &= B_0 + \frac{2}{3}C_0; \end{aligned} \quad (5)$$

and we decompose these into

$$X_0(r) = X_S(r) + X(r; \lambda); \quad (6)$$

where $X = A, B$, or C . Each X_S is defined by

$$\begin{aligned} A_S(r) &= \log \frac{3}{3 + \frac{3}{0}}; \\ B_S(r) &= \frac{2}{3} \log \left(1 + \frac{3}{0} \right); \\ C_S(r) &= 0; \end{aligned} \quad (7)$$

When we take $A = B = C = 0$ and $\lambda \rightarrow 1$ ($\lambda \rightarrow 1$), the 6D Schwarzschild solution in isotropic coordinates is recovered.

Black hole solutions are parameterized only by a parameter²

$$\lambda_0 = \frac{0}{\lambda}; \quad (8)$$

As we will see later (Fig. 6), the proper circumferential radius of the horizon on the brane is approximately equal to the parameter λ_0 . Black holes with $\lambda_0 < 1$ are small compared with the AdS curvature radius, whereas black holes with $\lambda_0 > 1$ are large.

B. Einstein equations

The Einstein equations yield five non-trivial equations. Three of them yield elliptic equations for the respective metric components $X = fA, B, Cg$,

$$(\partial_r^2 + \partial_z^2)X = S_X; \quad (9)$$

where the source S_X depends non-linearly on X and its derivatives. The remaining two equations give constraint equations, which satisfy Cauchy-Riemann relations. The Cauchy-Riemann relations are obtained from the non-trivial components of the Bianchi identities $r_{\mu\nu} = 0$, assuming that the equations for A, B , and C are satisfied. The Cauchy-Riemann relations in terms of f, g are

$$\frac{\partial^2}{\partial r^2} f - \frac{\partial^2}{\partial z^2} g = 0; \quad (10)$$

$$\frac{\partial^2}{\partial r^2} g - \frac{\partial^2}{\partial z^2} f = 0; \quad (11)$$

¹ The introduction of the variable λ is not essential in our numerics, but the increased resolution makes numerics work better, compared with calculations using the variable r . Indeed, this allows us to find larger black holes.

² In our numerical calculations, we take $\lambda_0 = 1$ and change λ to specify the parameter [26]. Because the variation of λ keeping λ_0 fixed corresponds to rescaling the length scale, we must be careful to compare physical quantities of a black hole to those of a black hole with different λ_0 . Thus in this paper we plot physical quantities in dimensionless form. We also note that physical size of the grid resolution (d, d_z) changes for each calculation due to the rescaling of the length scale, even if we fix the grid resolution.

where $\mathcal{E} := 2 \sqrt{\det g} G$, and $\mathcal{E} := \sqrt{\det g} (G - G)$: and are called weighted constraint equations. Since and satisfy Cauchy-Riemann relations, each of them satisfies Laplace equation. Hence if is satisfied on all boundaries and provided that vanishes at any one point, the two weighted constraints must vanish in all places as long as the elliptic equations for $A; B$, and C are satisfied.

C. Boundary conditions

To solve the elliptic equations (9) numerically, we need boundary conditions for them. The boundary conditions are determined by physical requirements. Let us first consider the boundary conditions on the event horizon. The horizon is a regular singular point of the elliptic equations for fixed . The regularity at the horizon demands that singular solutions should be absent. Thus a power expansion in of the elliptic equations and the constraint equation $(G - G) = 0$ results in boundary conditions at the horizon for regularity:

$$\partial A = \partial B = \frac{\cos}{z}; \quad \partial C = 0: \quad (\quad = 0) \quad (12)$$

In addition to these conditions, the regularity of the constraint equation $G = 0$ gives a condition

$$\partial (A - B + C) = 0: \quad (\quad = 0) \quad (13)$$

This additional requirement is physically a condition that temperature of a black hole is constant on the horizon (see Eq. (22)). We do not use this boundary condition for the elliptic equations, but we use it to integrate the constraint equation (see Sec. IIIA).

Boundary conditions on the brane are derived from the Israel's junction condition. They are given by

$$\begin{aligned} \partial A = \partial B &= -\frac{1}{\sqrt{}} \left(1 + \frac{3}{3} e^{B-C} \right); \quad (\quad = -2): \\ \partial C &= 0: \end{aligned} \quad (14)$$

On the axis $r = 0$, the absence of conical singularity requires

$$C(\quad; 0) = 0: \quad (15)$$

This condition is also required from the regularity of the equation for C on the axis. Furthermore, the axial symmetry requires that the r derivative of the metric functions vanishes on the axis. Thus we have

$$\partial A; \quad \partial B; \quad \partial C = 0: \quad (\quad = 0) \quad (16)$$

Let us consider the asymptotic boundary conditions. The background spacetime of the RS braneworld is the AdS spacetime. It is well known that localized matter fields reproduce linearized lower dimensional Einstein gravity on the brane in weak gravitational regime, and the linear perturbations fall off asymptotically keeping the spacetime to be asymptotically AdS. Thus in the current problem, we could assume that the spacetime is asymptotically AdS. Therefore, the asymptotic boundary conditions are

$$A; B; C = 0; \quad (\quad \rightarrow 1) \quad (17)$$

at spatial infinity, although in actual numerics these conditions are imposed at a finite coordinate location. In Appendix B, we discuss asymptotic behavior of gravitational field induced by a point mass on the brane. The gravitational field in the asymptotic region is anisotropic in the polar coordinates [6, 7, 54]. While the asymptotic behavior given by the point mass could provide asymptotic boundary conditions for the localized black holes as Neumann boundary conditions, we have not been able to find a stable scheme involving the boundary conditions. However, already with our simple implementation it is possible to derive interesting results as we will see (see Sec. IIIB for tests of our numerical method).

III. NUMERICAL SOLUTIONS

A. Stabilization of numerical scheme

In this section, we discuss the stability of our relaxation scheme of numerics. A problem of solving the elliptic equations (9) by a relaxation scheme is an instability coming from the axis ($r = 0$). A term in the equation for C

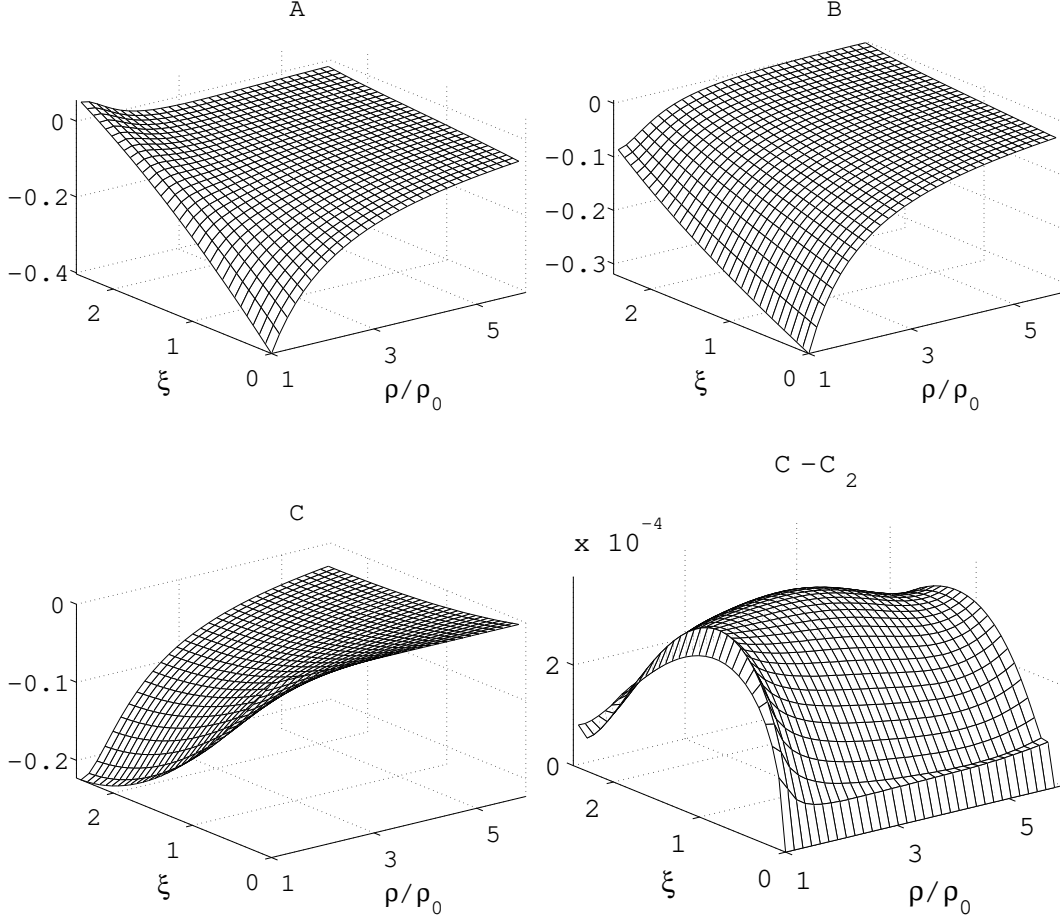


FIG. 1: Metric functions and $C - C_2$ for $\hat{\gamma}_0 = 0.5$.

	$h_j \bar{j}_l$		$h_j \bar{j}_l$		T		ξ		S_5	
	$\hat{\gamma}_0 = 0.5, 1.25$		$0.5, 1.25$		$0.5, 1.25$		$0.5, 1.25$		$0.5, 1.25$	
$m_{ax} = 6.0$	0.673	0.369	12.9	1.32	0.014	0.029	0.082	0.133	0.071	0.126
7.2	0.020	0.319	3.12	0.594	0.009	0.017	0.049	0.081	0.043	0.077
9.7	0.016	0.145	0.104	0.164	0.003	0.006	0.016	0.027	0.014	0.026
11.0	0.011	0.060	0.000	0.155	0.001	0.003	0.007	0.012	0.006	0.011

TABLE I: Table summarizing the sensitivity of the solutions to the finite position of the asymptotic boundary m_{ax} . In the table, we compare the temperature, entropy and weighted constraints, for solutions with $\hat{\gamma}_0 = 0.5$ and 1.25. The variation of the quantities is defined as $T = T_{(m_{ax}=12.2)} - 1$, dividing by T for $m_{ax} = 12.2$. The averaged absolute values of the weighted constraints, $h_j \bar{j}_l$ and $h_j \bar{j}_l$, are calculated for a fixed domain, $1 < \xi < 5$. The constraints appear to be even better satisfied as m_{ax} increases. Moreover thermodynamic quantities hardly change, indicating our choice of m_{ax} is sufficiently large. All solutions are at the same resolution as for 64 × 256 with $m_{ax} = 11.0$.

that has a factor $1=r^2$ gives severe contribution near the axis, and it invokes numerical instability [26]. Actually if we turn off the term during a calculation, then the calculation becomes very stable and converges to a solution, although the solution is not a solution of Einstein's equations. This issue of instability prevents us from finding large localized black holes in our previous work.

We deal with this term as in Ref. [22]. A second derivative term for C in the constraint equation $\nabla^2 C / G$ is simply $C_{,\xi\xi}$, and thus we can integrate it over the domain. A point is that this equation has no singular term as long as Eq. (16) is satisfied. Thus the solution for C integrated away from the axis has very good behavior near the axis. We call the solution C_2 to distinguish it from C. Given the characteristics we need two initial data surfaces, one at

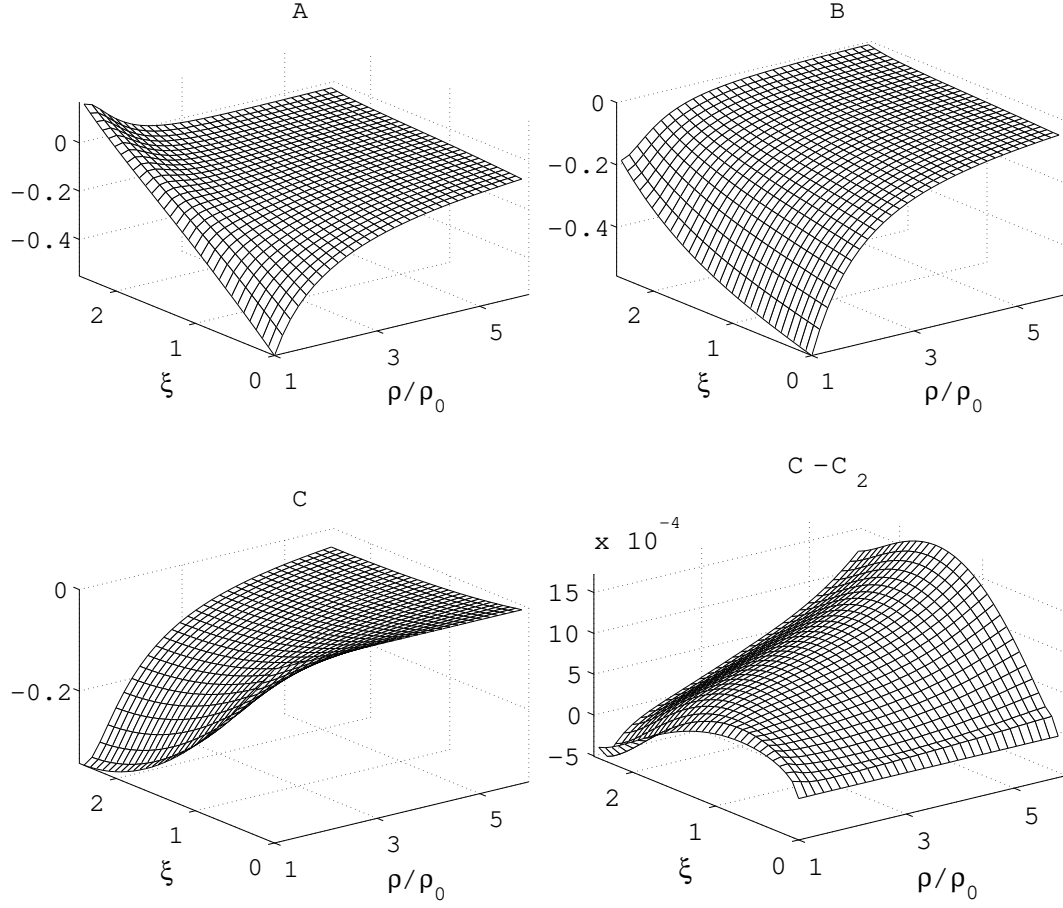


FIG .2: Metric functions and $C - C_2$ for $\gamma_0 = 1.25$.

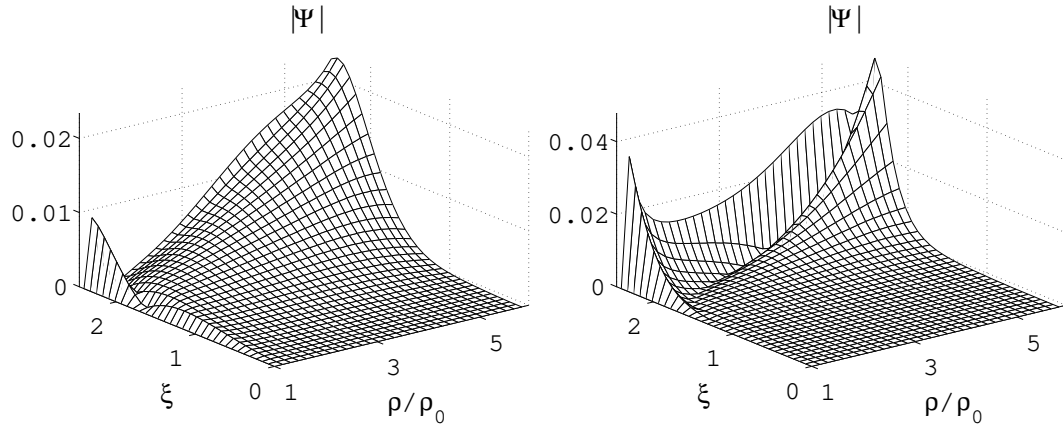


FIG .3: Absolute values of the weighted constraint equation for $\gamma_0 = 0.5$ (left) and $\gamma_0 = 1.25$ (right).

constant ρ , the other at constant ξ . Suitable surfaces are $\rho = 0$ and $\xi = 0$. For $\rho = 0$ we can set $C_2 = 0$ to satisfy the condition (15), and this ensures the good quality of the C_2 behavior near the axis. For the other initial surface $\xi = 0$, we fix C_2 using the condition (13) that the horizon temperature is a constant. We then integrate C_2 from

		$\hat{\gamma}_0 = 0.5$				$\hat{\gamma}_0 = 1.25$				C_2			
		h _j	j _i	h _j	j _i	h _j	j _i	h _j	j _i	h _j	j _i	h _j	j _i
32	128	4.1	10 ⁻²	3.4	10 ⁻¹	1.9	10 ⁻²	4.0	10 ⁻²	3.1	10 ⁻³	7.1	10 ⁻³
64	256	1.1	10 ⁻²	7.8	10 ⁻²	4.9	10 ⁻³	1.6	10 ⁻²	8.7	10 ⁻⁴	2.0	10 ⁻³
128	512	3.5	10 ⁻³	1.4	10 ⁻²	1.6	10 ⁻³	3.7	10 ⁻³	2.5	10 ⁻⁴	5.5	10 ⁻⁴

TABLE II: Table showing averaged violations of the absolute values of the weighted constraints and $C - C_2$ for the three resolutions. The three resolutions converge consistently with a second-order scaling. The averaged violations are calculated for a fixed domain $1 < r_0 < 5$.

these two boundaries.

$$\begin{aligned}
C_2(r; \gamma) &= \int_0^r dr' \int_{\gamma_0}^{\gamma} d\gamma' F(r', \gamma') + C(r; \gamma_0); \\
C(r; \gamma_0) &= (B(r) - A(r)) \gamma_0.
\end{aligned} \tag{18}$$

where F is the remaining terms in the constraint equation. We calculate the $1/r^2$ term in the elliptic equation for C using this function C_2 , rather than C . Then the term in question is replaced by

$$\frac{1}{r^2} \left(1 - e^{\frac{10}{3}C} \right) \rightarrow \frac{1}{r^2} \left(1 - e^{\frac{10}{3}C_2} \right). \tag{19}$$

This prescription dramatically improves stability of numerics, and we are free from the instability coming from the axis. Furthermore, we use the condition (13) in our scheme, the variation of the horizon temperature is vanishing small ($< 10^{-2}\%$), and the zeroth law of black hole thermodynamics is well satisfied.

B. Performance of the method

The formulations and numerical scheme described in the previous sections allow us to solve Einstein's equations as a boundary value problem. To solve the problem numerically, we use a relaxation method with a second order discretization scheme. In this section, we present some results of numerical calculations and discuss qualitative aspects of numerical solutions.

An illustration of metric functions for $\hat{\gamma}_0 = 0.5$ and $\hat{\gamma}_0 = 1.25$ are shown in Figs. 1 and 2. The former case is a typical for small localized black holes ($\hat{\gamma}_0 < 1$) and the latter case is for large localized black holes ($\hat{\gamma}_0 > 1$). As we see, the global behavior of metric functions hardly change for the two cases, but the peak values of metric functions increase, indicating that nonlinear effects become much more important for large black holes. It is remarkable that $C - C_2$ is very small, and then the integration method works consistently. We have performed the calculations for three different resolutions, 32 × 128, 64 × 256, 128 × 512 setting $d = d_0$. The finite position of the asymptotic boundary is at

$$r_{\text{max}} = 11 r_0. \tag{20}$$

In our simple implementation, largest horizon radius of a black hole that we could find depends on the resolution of the calculation, and then it is limited by computation time. The largest black hole that we found within a moderate computational time is $\hat{\gamma}_0 = 2$ with the grid resolution 128 × 512. The localized black holes are systematically constructed for the parameter region $\hat{\gamma}_0 = 0.002 - 2$.

Figure 3 shows absolute errors of the weighted constraint equation $\epsilon / (G - G_0)$. Because ϵ / G is essentially the same as ϵ due to the Cauchy-Riemann relations and we have confirmed the consistency of G by showing $C - C_2$ in Figs. 1 and 2, we suppress figures of ϵ . While the corresponding Einstein equation $G - G_0 = 0$ is well satisfied yielding vanishingly small values, peaks of the errors of the weighted constraints appear in the asymptotic region near the brane. The peaks are originated from the huge amplification of the tiny violations of Einstein's equations due to the weight function $\frac{1}{r^2}$ that is used to define ϵ . The weight function is proportional to r^{-5} near the brane. Because the tiny violation of Einstein's equations comes from the asymptotic boundary, we will need to avoid using the naive asymptotic boundary conditions (17). As we have discussed, the naive Dirichlet conditions could be replaced by appropriate Neumann conditions. The prescription will reduce such errors from finite boundary effects, if we can implement it without any numerical instability. Nevertheless, as r_{max} increases, the approximation using the

Dirichlet boundary conditions (17) becomes much better, and then violations of the weighted constraints decrease. This is observed in our numerics (Table I). The averaged absolute errors of the weighted constraints in a fixed domain, $\|h_j - \tilde{h}_j\|$ and $\|h_j - \tilde{h}_j\|$, decrease as m_{ax} increases. Thus, we do not care about the violations of the weighted constraints in the asymptotic region in the present numerics. In the Table I, we also show that errors from finite boundary effects in thermodynamic quantities are $\sim 1\%$ for Eq. (20), and then the location of the boundary is sufficiently far.

IV. PROPERTIES OF THE LOCALIZED BLACK HOLES

A. Thermodynamic quantities

We have demonstrated the numerical method and shown numerical examples of the localized black holes. The largest localized black hole that we found is $\hat{\alpha}_0 = 2$. In this section, we try to understand the properties of the localized black holes. Let us first consider thermodynamic quantities of the localized black holes. Thermodynamic quantities of interest are the horizon temperature T and the entropy S_6 of the black holes, which are given by

$$S_6 = \frac{1}{4G_6} \int_0^{\infty} d^3x \sqrt{-g} e^{4B_0 + C_0} \sin^3 \theta; \quad (21)$$

$$T = \frac{1}{2} \frac{3}{2^{5/3}} e^{A_0 + B_0 + C_0} \Big|_{r=r_h}; \quad (22)$$

In Fig. 4, we plot a thermodynamic relation between these quantities normalized by the AdS radius ℓ . The factor $G_6 = \ell^4$ is introduced to obtain correctly rescaled quantity (see footnote 2 in Sec. IIA). Three resolutions are used to generate the figures. One sees that they are consistent and compatible with second-order scaling. In the figure, we have also plotted the same thermodynamic relations for the 6D Schwarzschild black hole and the 6D black string, for comparison (see Appendix A). One finds that for sufficiently small horizon radius ($T \gg \ell^{-1}$), the thermodynamic relation of the localized black hole is a 6D Schwarzschild black hole type. This behavior is confirmed for the 5D localized black holes [27]. On the other hand, as the horizon radius increases ($T \ll \ell^{-1}$), the thermodynamic relation becomes a 6D black string type. The transition point at which the localized black hole changes its thermodynamic character is given by a temperature

$$T = \frac{1}{2\ell}; \quad (23)$$

As could be expected, this temperature is given by the temperature of the localized black hole with $\hat{\alpha}_0 = 1$, which is $T|_{\hat{\alpha}_0=1} = 0.9 = 2/\ell$. It is interesting that the horizon temperature (23) is the same as that of a 'critical' black string whose horizon radius r_h is $r_h = \ell$.

We consider the specific heat, $T dS_6 = dT$, of the localized black hole. It is immediately clear from Fig. 4 that the specific heat is negative. Because the temperature T and the entropy S_6 are well approximated by the 6D Schwarzschild black hole and the 6D black string in the respective regions ($T < \ell^{-1}$ and $T > \ell^{-1}$), the specific heat of the localized black hole is also well fitted by them.

There is an interesting quantity which characterizes the localized black hole by a geometrical quantity on the brane [27]. It is black hole 'entropy' measured by an observer living on the brane. We define the 5-dimensional entropy by using proper circumference at $z = \ell$ as

$$S_5 = \frac{1}{4G_5} \int_0^{\infty} d^3x \sqrt{-g} e^{3B_0 + 2C_0} \Big|_{z=\ell}; \quad (24)$$

In Fig. 4, we display a relation between S_5 and T taking an appropriate non-dimensional combination. In the figure, the same thermodynamic relations for the 6D black string and the 6D Schwarzschild black hole are also plotted for comparison. The figure shows that the 5-dimensional entropy S_5 deviates from that of the 6D Schwarzschild black holes as the temperature decrease. Then the entropy S_5 tends to behave like that of the 6D black string. Because of limited resolution and computing power, we could not confirm whether S_5 converges to the value of the 6D black string in the limit of large horizon radius ($T \rightarrow 0$). However, an extrapolation of our results for S_5 and S_6 suggests that the thermodynamic relations of the localized black hole converge to those of the 6D black string in the limit. Recall that the gravity induced on the brane by the 6D black string is the 5D Schwarzschild black hole. Therefore, if the convergence is true, it means that the gravity induced on the brane by the large localized black holes is well described by the 5D Einstein gravity. Thus, the above results imply that the recovery mechanism works even in the presence of the black hole which is not confined on the brane but localizes there, extending into the bulk.

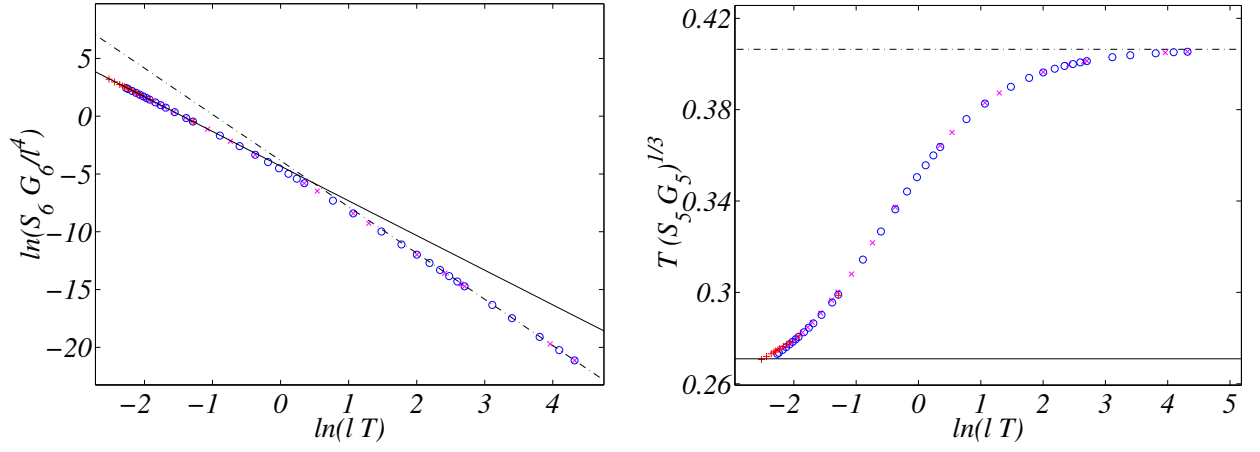


FIG. 4: Thermodynamic quantities of the localized black holes. The left figure shows a thermodynamic relation for the temperature T and the entropy S_6 which are normalized by the AdS curvature radius l . The right figure shows an appropriate combination of the 5D entropy S_5 and the temperature T as a function of the temperature. The thermodynamic relations for the 6D Schwarzschild black hole (dot-dashed line) and the 6D black string (solid line) are also plotted for a reference. To generate the figures, three resolutions are used, 32 (cross), 64 (circle), 128 (plus).

We give a comment on a possible deviation from the thermodynamic character of the black string. For the weak gravity regime in the original 5D braneworld model, the relative order of the Kaluza-Klein corrections to Newton's law is $O(l^2/r^2)$ [6, 7], where r is a coordinate radius. Similar Kaluza-Klein corrections will appear in the gravity induced on the brane by a black hole. However, the correction will be very small for massive black holes, and then numerical calculations can probe only the leading behavior. Therefore, even if numerical calculations show a good agreement between the thermodynamic character of the localized black hole and that of the black string, it does not mean that no correction to the 5D Schwarzschild black hole appears on the brane.

Mass of a black hole is an important quantity to characterize the black hole. If one assumes the first law of thermodynamics [47, 48], one can calculate a thermodynamic mass of a localized black hole. Because the localized black hole has the thermodynamic character analogous to those of the 6D Schwarzschild black hole and the 6D black string, the thermodynamic mass obtained by integrating the first law also agrees with them in the respective regime (Fig 5). The mass of large black holes is then approximated by that of the 6D black strings, neglecting small corrections coming from the integration over small radii. It is given by

$$M = \frac{1}{4} \frac{3}{\pi} S_6 \frac{l^{2=3}}{G_6} : (\hat{\alpha}_0 \approx 1) \quad (25)$$

The black hole entropy S_6 is greater than or nearly equal to that of the black string with the same mass. This is contrary to the argument for the (BTZ-like) localized black holes and the BTZ black strings in Ref. [48].

B. Horizon geometry and curvatures

A localized black hole is expected to have a flattened horizon geometry, and it will tend to flatten much more as its horizon radius increases [26, 27, 47]. Let us define polar and equatorial circumferential radii of the horizon by

$$\begin{aligned} R_{\text{eq}} &= r e^{B_0 + \frac{2}{3}C_0} \Big|_{z=0}; \\ R_{\text{polar}} &= \frac{4}{2} \frac{r_0}{0} \frac{z}{=2} \frac{d}{0} \frac{1}{z} e^{B_0 + C_0} : \end{aligned} \quad (26)$$

Figure 6 shows $R_{\text{eq}} = R_{\text{polar}}$ and R_{eq} . The small black holes are almost sphere $R_{\text{eq}} = R_{\text{polar}}$, but the large black holes show flattened geometry, $R_{\text{eq}} > R_{\text{polar}}$.

The intrinsic curvature of the horizon geometry gives us another information. The horizon 4-geometry is

$$d^2 = \frac{1}{z^2} e^{2(B_0 + C_0)} d^2 + r^2 e^{2B_0 + 4C_0} d^2 : \quad (27)$$

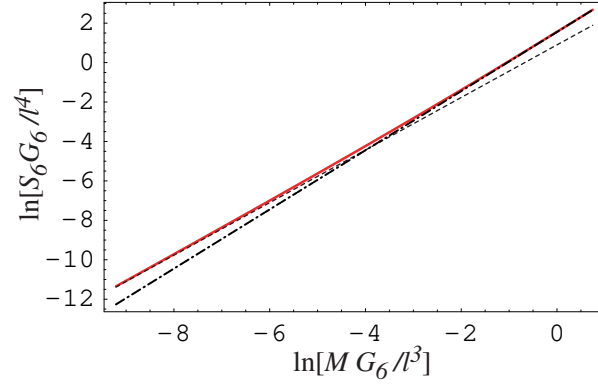


FIG . 5: The relation between the thermodynamic mass and the entropy for the localized black holes (solid curve). The dashed and the dot-dashed lines represent the relations for the 6D Schwarzschild black hole and the 6D black string, respectively.

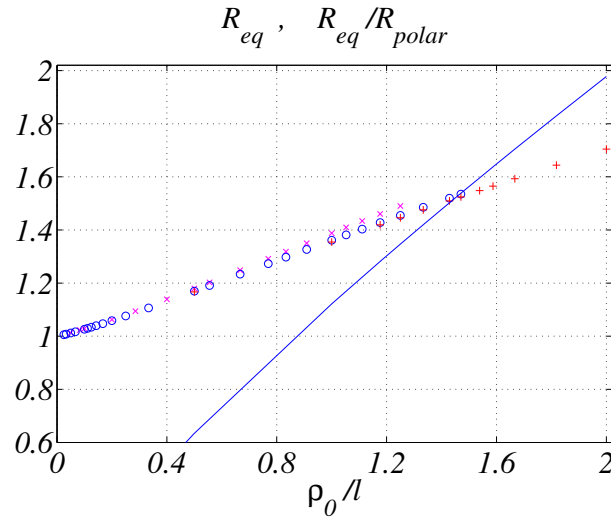


FIG . 6: Figure showing the ratio of the equatorial to polar circumferential radii for the localized black holes ($\gamma_0 = 2$). Three resolutions are used (32 \times 128 (cross), 64 \times 256 (circle), 128 \times 512 (plus)). The solid curve represents the equatorial radius R_{eq} with respect to γ_0 .

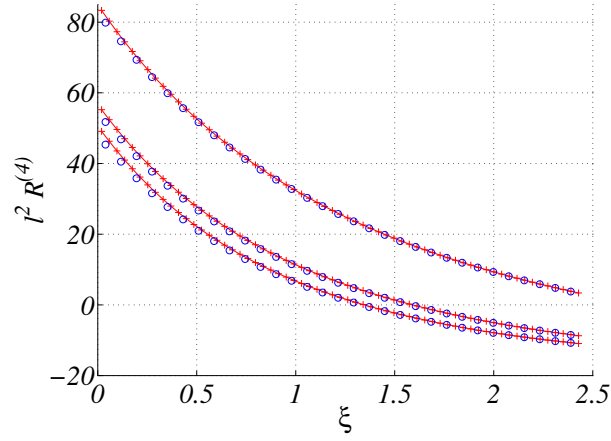


FIG . 7: Figure showing the intrinsic 4D curvatures $R^{(4)}$ of the horizon 4-geometry for $\gamma_0 = 0.5; 1; 1.4$. The curve showing the largest positive curvature on the axis $\xi = 0$ corresponds to $\gamma_0 = 0.5$. As the radius increases, the curvature on the axis decreases. While the curvature remains positive for $\gamma_0 = 0.5$, the curvature becomes negative near the brane for $\gamma_0 \geq 0.5$.

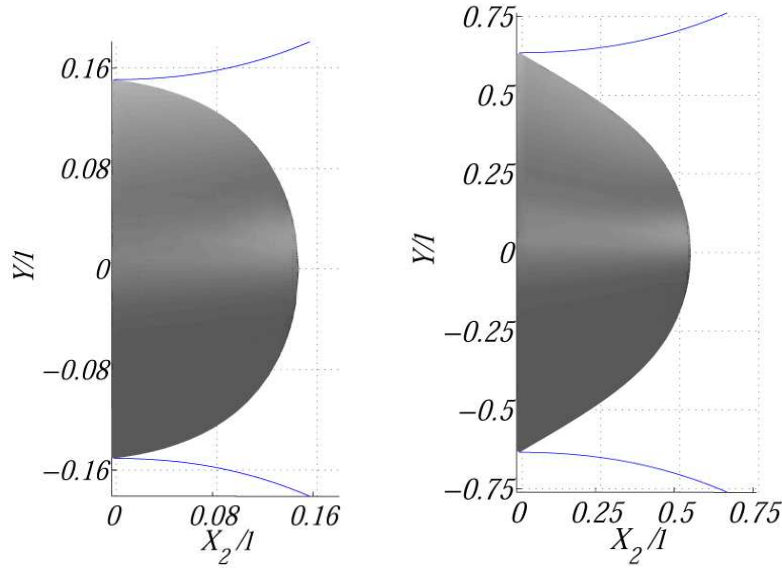


FIG. 8: The 4-geometry of the event horizon embedded in the Euclidean space (28), based on our numerical solutions. Two rotational degrees of freedom are suppressed. The size of the localized black holes in the left and right figures are $\hat{\alpha} = 0.1; 0.5$, respectively. The corresponding equatorial circumferential radii are $R_{eq} = 0.15, 0.63$, respectively. The solid curves show the location of the orbifold brane where the Z_2 -symmetry is imposed in the original space.

The 4D intrinsic curvature $R^{(4)}$ of the 4-geometry is shown in Fig. 7 for several black holes. The curvature becomes negative near the brane for the black holes with $\hat{\alpha} \lesssim 0.5$. The appearance of the negative spatial curvature near the brane is also confirmed for the EHM solution and the 6D black string (Appendix A). Because of this negative spatial curvature, embeddings of the spatial horizon geometry into a 5-dimensional Euclidean space

$$dE^2 = dX^2 + dY^2 + Y^2 d\frac{2}{3} \quad (28)$$

are not possible for all black holes, but only possible for small black holes (see e.g. [55]). The cylindrical and radial coordinates of the horizon are given by

$$X_{bh}(\theta) = \frac{Z}{d} \frac{S}{\frac{2}{3} \frac{d}{Z^2} e^{2(B_0 + C_0)} \frac{dY_{bh}^2}{d}}; \quad Y_{bh}(\theta) = \frac{r}{Z} e^{B_0 + \frac{2}{3}C_0}; \quad (29)$$

Figure 8 shows examples of the horizon geometry embedded in the Euclidean space. Because the cylindrical coordinate of the horizon on the axis does not coincide with the polar circumferential radius R_{polar} , the embeddings in the Euclidean space do not conserve the ratio $R_{eq} = R_{polar}$. To illustrate the horizon geometry, we rescale the cylindrical coordinate X for each black hole to conserve the ratio. The rescaled cylindrical coordinate is denoted by X_2 (Fig. 8). This illustration allows us to have an intuitive look of the horizon geometries for different horizon radii.

While we have compared the localized black hole to the black string, the black string has a curvature singularity at the AdS horizon as well as the ordinary singularity at the center of the event horizon (Appendix A) [28]. Thus the solution has been considered as an unphysical solution. Do the localized black holes have a naked singularity somewhere? To test the regularity of the spacetime, we calculate the square of the Riemann tensor that is one of curvature scalars,

$$K^{(6)} = R_{\mu\nu\rho\sigma} R^{\mu\nu\rho\sigma}; \quad (30)$$

It is hard to numerically calculate this kind of curvature scalars with enough accuracy near the axis and the horizon. In particular near the axis ($r = 0$), we encounter severe cancellations between terms that have coefficients proportional to $1/r^4, 1/r^3, \dots$. Nevertheless, we can confirm that the curvature $K^{(6)}$ is finite with good behavior. Then as far as the curvature $K^{(6)}$ is concerned, localized black holes have no naked singularity, at least in the computational domain. This supports that our localized black holes are physically acceptable black hole solutions. In Fig. 9, we illustrate

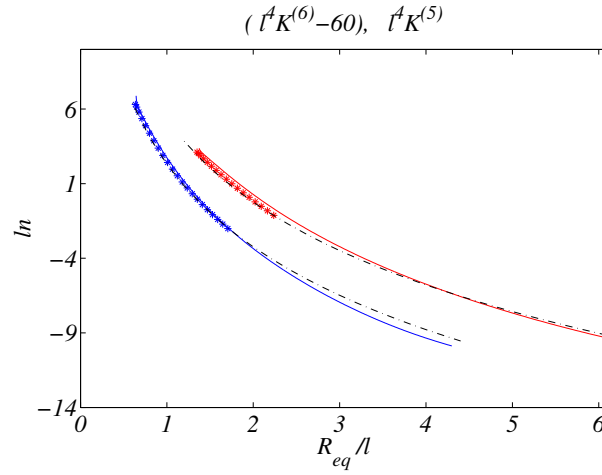


FIG. 9: Figure showing the 6D and 5D square of Ricciann curvature, $\ln(l^4 K^{(6)} - 60)$ (asterisk) and $\ln(l^4 K^{(5)})$ (solid curve), on the brane for $\gamma_0 = 0.5; 1.25$. The dot-dashed curves show fits to the asymptotic behavior §3).

the curvature $K^{(6)}$ on the brane. It goes rapidly to a constant value given by the AdS_6 ,

$$K^{(6)} = \frac{60}{v_4}; \quad (\text{AdS}_6) \quad (31)$$

and then it begins to fluctuate due to round-off error. Thus in Fig 9, we show $K^{(6)}$ for an appropriate range of proper circumferential radius R_{eq} on the brane. We have furthermore calculated the square of the 5D Ricciann tensor

$$K^{(5)} = R^{(5)} - R^{(5)}; \quad (32)$$

by using the induced metric on the brane. This curvature is a good measure for an observer on the brane. The scalar curvature for the 5D Schwarzschild black hole is

$$K^{(5)} = \frac{1}{R_{\text{eq}}^8}; \quad (33)$$

at a distance from the horizon (see Eq. (A 3)). On the other hand, the curvature $K^{(5)}$ for the 6D Schwarzschild black hole is proportional to $1/R_{\text{eq}}^{10}$. We could then compare these behavior with that of the curvature for the localized black holes. We plot $K^{(5)}$ of the localized black holes with $\gamma_0 = 0.5$ and 1.25 in Fig. 9. The dot-dashed curves are fits for the form §3) in an appropriate asymptotic region. Although the localized black hole with $\gamma_0 = 1.25$ is not so large, we observe that the 5D curvature for $\gamma_0 = 1.25$ shows better agreement with Eq. (33), compared to that for the smaller black hole. We note that the fit to the behavior §3) is better than a fit to the behavior $1/R_{\text{eq}}^{10}$. However we refrain from going into a discussion of such asymptotic behavior, because the asymptotic boundary conditions adopted in this paper are too naive to discuss it.

V. CONCLUSION

No realistic black holes localized on the brane have been found so far in the warped compactification, except for the EHM solutions in the 4-dimensional braneworlds. Black holes are important physical objects to understand and to test strong gravitational phenomena in the warped compactification. We have explored this problem by means of numerics, constructing black holes localized on the brane. We have employed the conformal gauge method that has been developed to study relativistic stars on the brane, non-uniform black strings and Kaluza-Klein black holes. In our previous work, we could not succeed in constructing large black holes, but could construct only the small black holes ($\gamma_0 \lesssim 1$). However improved numerics allow us to construct the large localized black holes with $\gamma_0 \gtrsim 1$, and then we have studied the properties of the localized black holes.

The largest size of the black holes that could be relaxed in a reasonable computational time is $\gamma_0 = 2$ in this paper. The parameter γ_0 is approximately equal to the proper circumferential radius on the brane. The largest size depends

on the resolution of the calculation, and thus it is limited by the computational time. The situation would be similar to the study of the large relativistic stars [19].

The horizon geometry of the localized black holes is flattened in the bulk. The ratio of the equatorial to polar circumferential radii shows that the localized black hole becomes much more flattened as its horizon radius increases (Fig. 6). We have pointed out that the intrinsic curvature of the horizon 4-geometry becomes negative near the brane for the black holes with $\hat{\alpha}_0 < 0.5$. Then the global shape of the flattened horizon changes as its horizon radius increases.

The thermodynamic properties of the localized black holes have been discussed by investigating the entropy, temperature and specific heat of the black holes. For the small black holes ($\hat{\alpha}_0 < 1$) the thermodynamic relation between the entropy and the temperature is the 6D Schwarzschild black hole type, whereas for the large black holes ($\hat{\alpha}_0 > 1$) the thermodynamic relation is the 6D black string type (Fig. 4). The transition occurs at $T = 1/2$, corresponding to $\hat{\alpha}_0 = 1$. The 5D entropy measured by an observer on the brane also shows the transition: the physical quantities of the large localized black holes are approximately described by the 6D black strings. Thus the large localized black hole looks like the 6D black string with its ends capped off. This transition of thermodynamic relations might be analogous to an expected transition between a sequence of (static) black string solutions and that of black hole solutions in the Kaluza-Klein compactification [56], although the transition is questioned by the recent study [22].

Recall that the induced gravity of the 6D black string is given by the 5D Schwarzschild black hole. Then the above results indicate that the gravity induced on the brane by the large localized black hole is approximated by the 5D Einstein gravity. Such recovery mechanism of lower dimensional Einstein gravity on the brane is proved in the weak gravity regime by means of linear and second-order perturbations [7, 12], and it is partially confirmed for the strong gravity regime by the numerical study [19]. Our result also suggests that the recovery mechanism works even in the presence of the black hole that is bound to the brane.

Let us discuss the relation between our results and the argument of the classical black hole evaporation conjecture [52, 53]. The argument claims that large localized static black holes may not exist. On one hand, the physical quantities calculated in this paper have not indicated a critical point at which a sequence of solutions suddenly disappears or some kind of singular behavior appears. Then it seems to shed doubts on the conjecture. On the other hand, however, the largest localized black hole in this paper is $\hat{\alpha}_0 = 2$, and the black hole is not sufficiently large. It would be still small compared with the black holes supposed in the conjecture. It is certainly true that we cannot provide a conclusive disproof (or proof) of the conjecture by means of numerics, even if we construct a very large black hole with, e.g., $\hat{\alpha}_0 = 100$. In Ref. [27], some possible consistent scenarios are discussed. However, we expect that the sequence of our localized black holes represents the unique stable vacuum solution without naked singularity that describes a nonrotating uncharged black hole bound to the brane. Needless to say, it is preferable to have an analytic solution of a localized black hole, and thus much progress in the study of braneworld black holes is required.

An interesting application of the conformal gauge method is a study of black holes in the RS two-branes model. Because the localized black holes in the model are similar to black holes in the Kaluza-Klein compactification, the method in Ref. [22] can be directly applied. Effects of the warped compactification, the second brane and radius stabilization mechanism on the black holes would result in different phenomena observed in this paper. Charged localized black holes are also interesting. Introducing gauge fields on the brane is not difficult in our approach. We hope to report soon our results toward these directions.

Acknowledgments

The author would like to thank Hideo Kodama, Takahiro Tanaka, Toby Wiseman and Bruce Bassett for their valuable comments and discussions. The author is grateful to Toby Wiseman for his hospitality at Cambridge. The numerical computations reported in this work were carried out at the Yukawa Institute Computer Facility and at the NAO. This work is supported in part by the JSPS and a Grant-in-Aid for the 21st Century COE.

APPENDIX A : 6D BLACK STRING

Black string solution in the single brane model has a singularity at the AdS horizon ($z \rightarrow 1$) [28]. However, the solution is still useful as a reference. The 6D black string is given by

$$ds^2 = \frac{v^2}{z^2} \left(-V dt^2 + V^{-1} dr^2 + r^2 d\Omega_3^2 + dz^2 \right); \quad (\text{A } 1)$$

where $V = 1 - \frac{r^2}{r_h^2}$. The brane is at $z = 1$. The square of the Riemann tensor is

$$K^{(6)} = R_{\mu\nu} R^{\mu\nu} = \frac{1}{z^4} \left(60 + \frac{72r_h^4 z^4}{r^8} \right); \quad (\text{A } 2)$$

which diverges at the AdS horizon ($z \rightarrow 1$), as well as at the black string singularity at $r = 0$. The 5D curvature scalar (32) on the brane is given by

$$K^{(5)} = 72r_h^4 = r^8; \quad (\text{A } 3)$$

The intrinsic curvature $R^{(4)}$ of the horizon 4-geometry is

$$R^{(4)} = \frac{6}{r_h^2 z^2} (z^2 - 2r_h^2); \quad (\text{A } 4)$$

This is not always positive, but becomes negative for $z < \sqrt{2}r_h$.

Temperature and entropy of the black string are

$$\begin{aligned} T &= \frac{1}{2r_h}; \\ S_6 &= \frac{1}{4G_6} \frac{(2r_h)^2}{3} r_h^3; \end{aligned} \quad (\text{A } 5)$$

Assuming the first law, thermodynamic mass is given by $M = \frac{1}{4} \frac{S_6^2}{G_6} = \frac{1}{4} \frac{S_6^2}{G_6} = \frac{1}{4} \frac{S_6^2}{G_6}$.

APPENDIX B: ASYMPTOTIC BOUNDARY CONDITIONS

1. Linear perturbations

Asymptotic behavior of black hole characterizes the black hole itself, and then it is important. To impose physically reasonable asymptotic boundary conditions, we need to solve linear perturbations of the black hole geometry in the asymptotic region. Here we assume that the asymptotic behavior of black hole geometry is equivalent to that of gravitational field induced by a point mass on the brane. Then we consider solutions to the linear perturbations of weak gravitational field in the conformal gauge. Linearized equations in the conformal gauge do not yield decoupled equations, and then it is difficult to solve it. However using the transverse-traceless gauge, one finds that a master equation exists and it is solved using Green's function. The discussion in this appendix is based on an argument in Ref. [19].

Perturbations in the transverse-traceless (TT) gauge are given by

$$ds^2 = \frac{z^2}{z^2} \left(e^{2F} dt^2 + e^{2H} dr^2 + r^2 e^{2D} d\Omega^2 + dz^2 \right); \quad (\text{B } 1)$$

where F and D are determined by the TT conditions,

$$F = \frac{1}{r^3} \partial_r (r^4 H); \quad D = \frac{1}{3r^2} \partial_r (r^3 H); \quad (\text{B } 2)$$

Linearized equation for H is given by

$$0 = \frac{z^2}{z^2} \left(\partial_r^2 + \frac{5}{r} \partial_r + \partial_z^2 - \frac{4}{z} \partial_z \right) H; \quad (\text{B } 3)$$

Comparing these coordinates to those in the conformal gauge, coordinate transformations to bring the metric into the conformal gauge are $r_{TT}^0 = r + f$, $z_{TT}^0 = z + g$ with $g_{,z} = f_{,r} + H$; $g_{,r} = -f_{,z}$ which yield Poisson equations for f and g [19],

$$4\Box g = H_{,z}; \quad 4\Box f = -H_{,r}; \quad (\text{B } 4)$$

$$f(r; z) = f_p \int_0^z \frac{1}{q} \sin(qr) e^{qz} dq : \quad (\text{B } 11)$$

From the boundary condition $3\partial_r g = -r\partial_z H$ on the brane, we obtain

$$F(q) = \frac{2h_0}{3} + \frac{8h_0}{3} e^q [2K_0(q) - qK_1(q)] : \quad (\text{B } 12)$$

On the brane ($z = 0; r = r$), the leading order contributions are evaluated as

$$\begin{aligned} g &= \frac{h_0}{3r^2}; \\ f &= \frac{h_0}{r} O(\log(r)) : \end{aligned} \quad (\text{B } 13)$$

Near the axis ($z = 0, r = 0$), we have

$$\begin{aligned} g &= O\left(\frac{\log z}{z}\right); \\ f &= \frac{rh_0}{z} O\left(\frac{1}{z}\right) + O\left(\frac{\log z}{z}\right) : \end{aligned} \quad (\text{B } 14)$$

The coordinate transformation (B 11) and the asymptotic behavior (B 9) (or the solution in Ref. [54]) with Eq. (B 5) can be used as the asymptotic boundary condition of localized black holes.

-
- [1] L. Randall and R. Sundrum, Phys. Rev. Lett. 83, 3370 (1999), hep-ph/9905221.
 - [2] L. Randall and R. Sundrum, Phys. Rev. Lett. 83, 4690 (1999), hep-th/9906064.
 - [3] N. Arkani-Hamed, S. Dimopoulos, and G. R. Dvali, Phys. Lett. B 429, 263 (1998), hep-ph/9803315.
 - [4] I. Antoniadis, N. Arkani-Hamed, S. Dimopoulos, and G. R. Dvali, Phys. Lett. B 436, 257 (1998), hep-ph/9804398.
 - [5] T. Shiromizu, K. Maeda, and M. Sasaki, Phys. Rev. D 62, 024012 (2000), gr-qc/9910076.
 - [6] M. Sasaki, T. Shiromizu, and K. Maeda, Phys. Rev. D 62, 024008 (2000), hep-th/9912233.
 - [7] J. Garriga and T. Tanaka, Phys. Rev. Lett. 84, 2778 (2000), hep-th/9911055.
 - [8] T. Tanaka and X. Montes, Nucl. Phys. B 582, 259 (2000), hep-th/0001092.
 - [9] S. Mukohyama, Phys. Rev. D 65, 084036 (2002), hep-th/0112205.
 - [10] S. Mukohyama and L. Kofman, Phys. Rev. D 65, 124025 (2002), hep-th/0112115.
 - [11] I. Giannakis and H.-c. Ren, Phys. Rev. D 63, 024001 (2001), hep-th/0007053.
 - [12] H. Kudoh and T. Tanaka, Phys. Rev. D 64, 084022 (2001), hep-th/0104049.
 - [13] H. Kudoh and T. Tanaka, Phys. Rev. D 65, 104034 (2002), hep-th/0112013.
 - [14] H. Kudoh and T. Tanaka, Phys. Rev. D 67, 044011 (2003), hep-th/0205041.
 - [15] T. Wiseman, Class. Quant. Grav. 19, 3083 (2002), hep-th/0201127.
 - [16] S. Kanno and J. Soda, Phys. Rev. D 66, 083506 (2002), hep-th/0207029.
 - [17] T. Shiromizu and K. Koyama, Phys. Rev. D 67, 084022 (2003), hep-th/0210066.
 - [18] J. Martin, G. N. Felder, A. V. Frolov, M. Peloso, and L. Kofman (2003), hep-th/0309001.
 - [19] T. Wiseman, Phys. Rev. D 65, 124007 (2002), hep-th/0111057.
 - [20] T. Wiseman, Class. Quant. Grav. 20, 1137 (2003), hep-th/0209051.
 - [21] T. Wiseman, Class. Quant. Grav. 20, 1177 (2003), hep-th/0211028.
 - [22] H. Kudoh and T. Wiseman (2003), hep-th/0310104.
 - [23] E. Sorkin, B. Kol, and T. Piran (2003), hep-th/0310096.
 - [24] M. A. L. L. et al., Int. J. Mod. Phys. D 10, 273 (2001), gr-qc/9908012.
 - [25] M. Shibata, Prog. Theor. Phys. 104, 325 (2000), gr-qc/0007049.
 - [26] H. Kudoh, T. Tanaka, and T. Nakamura, Phys. Rev. D 68, 024035 (2003), gr-qc/0301089.
 - [27] H. Kudoh, Prog. Theor. Phys. 110, 1059 (2004), hep-th/0306067.
 - [28] A. Chamblin, S. W. Hawking, and H. S. Reall, Phys. Rev. D 61, 065007 (2000), hep-th/9909205.
 - [29] A. Chamblin, H. S. Reall, H.-a. Shinkai, and T. Shiromizu, Phys. Rev. D 63, 064015 (2001), hep-th/0008177.
 - [30] C. Cadeau and E. W. Olgar, Class. Quant. Grav. 18, 527 (2001), gr-qc/0011029.
 - [31] R. Casadio and L. Mazzacurati, Mod. Phys. Lett. A 18, 651 (2003), gr-qc/0205129.
 - [32] R. Casadio, A. Fabbri, and L. Mazzacurati, Phys. Rev. D 65, 084040 (2002), gr-qc/0111072.
 - [33] N. Dadhich, R. M. aartens, P. Papadopoulos, and V. Rezanian, Phys. Lett. B 487, 1 (2000), hep-th/0003061.
 - [34] I. Giannakis and H.-c. Ren, Phys. Rev. D 63, 125017 (2001), hep-th/0010183.
 - [35] M. S. Modgil, S. Panda, and G. Sengupta, Mod. Phys. Lett. A 17, 1479 (2002), hep-th/0104122.

- [36] P. Kanti and K. Tamvakis, Phys. Rev. D 65, 084010 (2002), hep-th/0110298.
- [37] G. Konas, E. Papantonopoulos, and V. Zamarias, Phys. Rev. D 66, 104028 (2002), hep-th/0208207.
- [38] H. Kodama, Prog. Theor. Phys. 108, 253 (2002), gr-qc/0204042.
- [39] S. Shankaranarayanan and N. Dadhich (2003), gr-qc/0306111.
- [40] T. Tamaki, S. Kanno, and J. Soda (2003), hep-th/0307278.
- [41] S. I. Vacaru and E. Gaburov (2001), hep-th/0108065.
- [42] S. I. Vacaru (2001), hep-th/0110250.
- [43] C. Charmousis and R. Gregory, Class. Quant. Grav. 21, 527 (2004), gr-qc/0306069.
- [44] P.-J. De Smet, Class. Quant. Grav. 20, 2541 (2003), gr-qc/0302081.
- [45] K. T. P. Kanti, I. O. Lasagasti (2003), hep-th/0307201.
- [46] P. S. D. Karasik, C. Sahabandu and L. C. R. Wijewardhana (2003), gr-qc/0309076.
- [47] R. Emparan, G. T. Horowitz, and R. C. Myers, JHEP 01, 007 (2000), hep-th/9911043.
- [48] R. Emparan, G. T. Horowitz, and R. C. Myers, JHEP 01, 021 (2000), hep-th/9912135.
- [49] M. Buni, C. Gernani, and R. M. aartens, Phys. Rev. Lett. 87, 231302 (2001), gr-qc/0108013.
- [50] M. J. Du and J. T. Liu, Phys. Rev. Lett. 85, 2052 (2000), hep-th/0003237.
- [51] S. W. Hawking, T. Hertog, and H. S. Reall, Phys. Rev. D 62, 043501 (2000), hep-th/0003052.
- [52] R. Emparan, A. Fabbri, and N. Kaloper, JHEP 08, 043 (2002), hep-th/0206155.
- [53] T. Tanaka, Prog. Theor. Phys. Suppl. 148, 307 (2003), gr-qc/0203082.
- [54] S. B. Giddings, E. Katz, and L. Randall, JHEP 03, 023 (2000), hep-th/0002091.
- [55] C. Misner, K. Thorne, and J. Wheeler, Gravitation (Freeman, 1973).
- [56] B. Kol (2002), hep-th/0206220.